Schéma à capture de choc et multirésolution adaptative pour la simulation d'écoulements visqueux compressibles

Christian TENAUD [1],
Yann FRAIGNEAU [1] and Virginie DARU [1,2]

[1] LIMSI - CNRS UPR 3251, Orsay, France;
[2] Laboratoire Dynfluid - Arts et Métiers ParisTech, Paris XIII, France.

IHP Paris; 5th – 6th July 2011

Introduction

Predictions of compressible flows / multiple time and length scales.

- **Increase of computer power:** D.N.S. a powerful tool for fine analysis of flow dynamics.
- **Quality of results:**
  - ability of approximations: Capture small scale structures / discontinuities;
  - ability of computational grid to capture length scales.

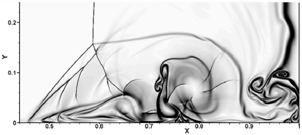

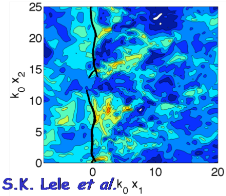

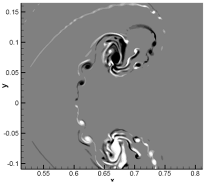

Flame front; diphasic interface; shock/Turbulence interaction; vorticity production by baroclinic effect: need High-order schemes + mesh refinement.

Vorticity production by baroclinic effect: Shock / hot bubble interaction.

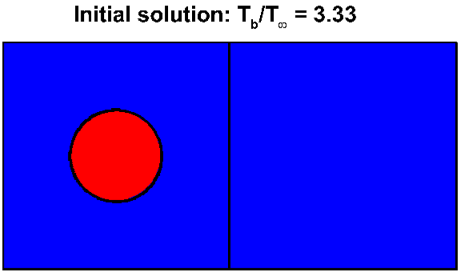

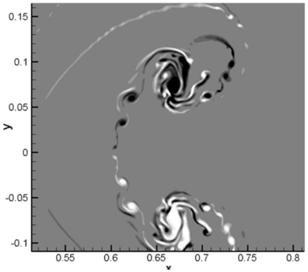

Vorticity production by baroclinic effect: video of the solution

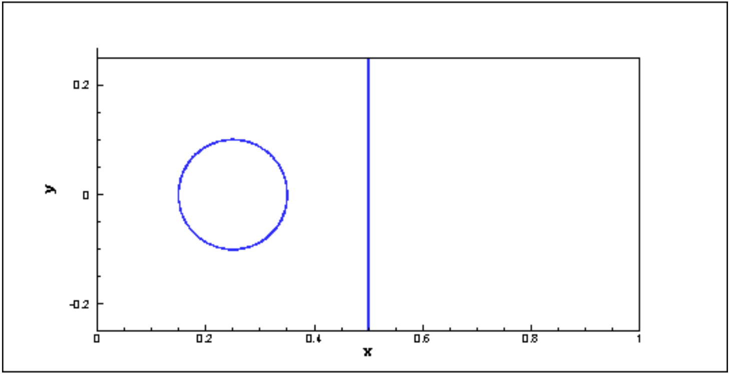

Shock / hot bubble interaction: density countours.

Vorticity production by baroclinic effect: video of the adapted grid

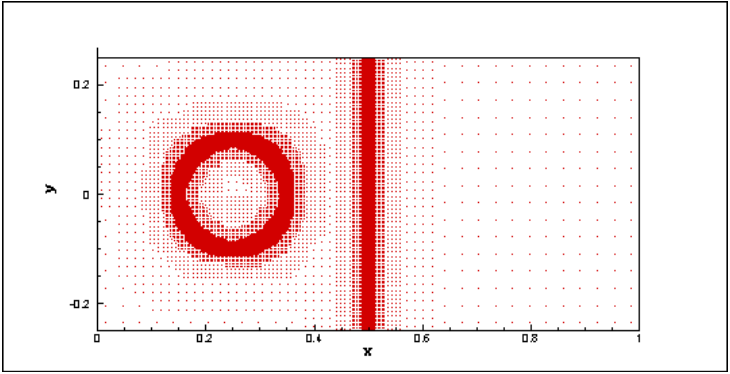

Shock / hot bubble interaction: adapted grid using 9 grid levels.

Objectives of the presentation

- System of equations;
- Numerical approximation **OSMPx** [V. Daru & C. Tenaud, 2001, 2004];
  - Lax-Wendroff approach;
  - Shock capturing features (TVD, MP);
- Adaptive MultiResolution technique [A. Harten, 1994 ; A. Cohen, 2003];
  - Multiscale decomposition;
  - Adaptive MR formalism: wavelet basis;
- Couple OSMPx / adaptive MR. Influence on accuracy, CPU time consumption, memory usage, evaluated on well known test-cases:
  - Hyperbolic conservation laws: linear and nonlinear scalar transport equation,
  - Euler and Navier-Stokes solutions in 1-, 2- and 3-D.
- Conclusion and prospect.

Conservation Law: equations

$$\left\{ \begin{array}{ll} \dfrac{\partial \mathbf{w}}{\partial t} + \nabla \cdot \mathbf{f}(\mathbf{w}, \nabla \mathbf{w}) = \mathbf{S}(\mathbf{w}) & \text{in } \Omega, t \in \mathbb{R}^+ \\ \mathbf{w}(\mathbf{x}, 0) = \mathbf{w}_0(\mathbf{x}), & \\ \mathbf{w}(\mathbf{x}, t) = \mathbf{g}(\mathbf{x}, t) & \text{on } \partial\Omega. \end{array} \right. \tag{1}$$

$$\mathbf{w}(\mathbf{x}, t) = \begin{pmatrix} \rho \\ \rho\, \mathbf{u} \\ \rho\, E \end{pmatrix} \tag{2}$$

$$\mathbf{f}(\mathbf{w}, \nabla \mathbf{w}) = \begin{pmatrix} \rho\, \mathbf{u} \\ \rho\, \mathbf{u} \otimes \mathbf{u} + \dfrac{P}{\gamma \mathrm{M}^2} \mathbb{I} \\ \rho\, \mathbf{u}\, E + \mathbf{u}\, P \end{pmatrix} - \frac{\mu}{\mathrm{Re}} \begin{pmatrix} 0 \\ \tau = \nabla \mathbf{u} + \nabla^t \mathbf{u} - \dfrac{2}{3} \nabla \cdot \mathbf{u} \\ \mathbf{u} \cdot \tau - \dfrac{1}{(\gamma - 1) \mathrm{Pr}\, \mathrm{M}^2} \nabla T \end{pmatrix} \tag{3}$$

$$P = P(\rho, e) = \rho\, T \tag{4}$$

Conservation Law: computational domain

Domain: dense partition of Ω into N_0 intervals of size h_0;

$$\Omega = \bigcup_{j \in [0, N_0]} V_j^0 \;\; ; \;\; \text{with } \left| V_j^0 \bigcap V_k^0 \right| = 0 \;\text{ for } j \neq k; \;\; j, k \in [0, N_0].$$

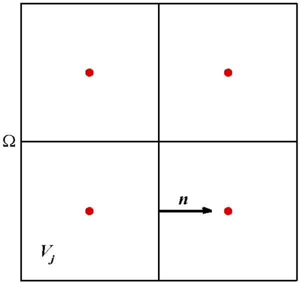

Conservation Law: computational domain

Domain: dense partition of Ω into N_0 intervals of size h_0;

$$\Omega = \bigcup_{j \in [0, N_0]} V_j^0 \quad ; \quad \text{with } \left| V_j^0 \bigcap V_k^0 \right| = 0 \ \text{ for } j \neq k; \ j, k \in [0, N_0].$$

Looking for successive approximations $(\mathbf{w}_j)^n$ of the average value of $\mathbf{w}(\mathbf{x}, t)$ in control volumes, at time $n\,\delta t$:

$$(\mathbf{w}_j)^n = \frac{1}{|V_j^0|} \int_{V_j^0} \mathbf{w}(\mathbf{x}, n\,\delta t)\, d\mathbf{x}$$

where $|V_j^0| = \int_{V_j^0} d\mathbf{x}$

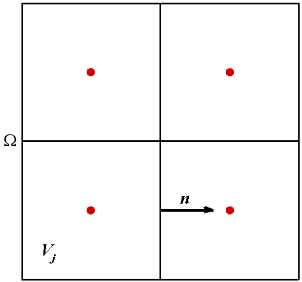

Conservation Law: Finite-Volume approach

$$(\mathbf{w}_j)^n = \frac{1}{|V_j^0|}\int_{V_j^0} \mathbf{w}(\mathbf{x}, n\,\delta t)\, d\mathbf{x}\ ;\ |V_j^0| = \int_{V_j^0} d\mathbf{x}$$

$$\int_{n\delta t}^{(n+1)\delta t}\int_{V_j^0}\left(\frac{\partial \mathbf{w}}{\partial t} + \nabla\cdot\mathbf{f}(\mathbf{w},\nabla\mathbf{w})\right)\, d\mathbf{x}\, dt = 0.$$

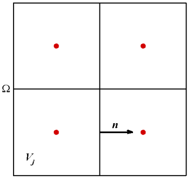

$$\mathbf{w}_j^{(n+1)} = \mathbf{w}_j^{(n)} - \sum_{m=1}^{N_{dim}} \frac{\delta t}{\delta x_m}\left(\overline{F}^n_{m,j+1/2} - \overline{F}^n_{m,j-1/2}\right)$$

Numerical flux: $2p$ grid points

$$\overline{F}^n_{m,j+1/2}(\mathbf{w}^n_{j-p+1}, \ldots\mathbf{w}^n_j, \ldots\mathbf{w}^n_{j+p}) = \int_{n\delta t}^{(n+1)\delta t}\int_{\partial V_j^0} \mathbf{f}(\mathbf{w},\nabla\mathbf{w})\cdot\mathbf{n}\; d\sigma\; dt$$

Overview

- System of equations;
- Numerical approximation **OSMPx** [V. Daru & C. Tenaud, 2001, 2004];
  - Lax-Wendroff approach;
  - Shock capturing features (TVD, MP);
- Adaptive MultiResolution technique [A. Harten, 1994 ; A. Cohen, 2003];
  - Multiscale decomposition;
  - Adaptive MR formalism: wavelet basis;
- Couple OSMPx / adaptive MR. Influence on accuracy, CPU time consumption, memory usage, evaluated on well known test-cases:
  - Hyperbolic conservation laws: linear and nonlinear scalar transport equation,
  - Euler and Navier-Stokes solutions in 1-, 2- and 3-D.
- Conclusion and prospect.

Approximation: **OS** basis scheme

$$\frac{\partial w}{\partial t} + \frac{\partial f(w)}{\partial x} = 0 \quad \text{with} \quad f(w) = a\,w\ (a > 0)$$

Lax-Wendroff scheme

$$w_j^{n+1} = w_j^n - \frac{\delta t}{\delta x}\left(F_{j+1/2}^{lw} - F_{j-1/2}^{lw}\right) \tag{5}$$

with the Lax-Wendroff numerical flux:

$$F_{j+1/2}^{lw} = f_j^n + \frac{(1-\nu)}{2}\left(f_{j+1}^n - f_j^n\right) \quad \text{CFL number} \quad \nu = a\frac{\delta t}{\delta x}.$$

Modified equation:

$$u_t + f(u)_x = a\frac{\delta x^2}{6}(\nu^2 - 1)u_{xxx} \tag{6}$$

Approximation: **OS** basis scheme

3rd order One Step scheme: OS3

$$F^3_{j+1/2} = f^n_j + \frac{(1-\nu)}{2}\left(f^n_{j+1} - f^n_j - \frac{1+\nu}{3}\left(f^n_{j+1} - 2f^n_j + f^n_{j-1}\right)\right) \tag{7}$$

Numerical flux recasts in a 3-point like scheme:

$$F^3_{j+1/2} = f^n_j + \Phi^3_{j+1/2}\frac{(1-\nu)}{2}\left(f^n_{j+1} - f^n_j\right) \tag{8}$$

with

$$\Phi^3_{j+1/2} = 1 - \frac{1+\nu}{3}\left(1 - r_{j+1/2}\right) \tag{9}$$

$$r_{j+1/2} = \frac{u^n_j - u^n_{j-1}}{u^n_{j+1} - u^n_j}.$$

Approximation: o-th order **OSo** scheme

o-th order One Step scheme: OSo

$$w_j^{n+1} = w_j^n - \frac{\delta t}{\delta x}(F^o_{j+1/2} - F^o_{j-1/2}) \tag{10}$$

$$F^o_{j+1/2} = f_j^n + \Phi^o_{j+1/2}\frac{(1-\nu)}{2}(f^n_{j+1} - f^n_j) \tag{11}$$

Function $\Phi^o_{j+1/2}$ drives the *o*-th order of accuracy of the scheme.

$$\Phi^4_{j+1/2} = \Phi^3_{j+1/2} + \frac{1+\nu}{3}\cdot\frac{\nu-2}{4}(1 - 2\ r_{j+1/2} + r_{j+1/2}\ r_{j-1/2}) \tag{12}$$

....

$$\begin{aligned}\Phi^7_{j+1/2} \quad = \quad & \Phi^6_{j+1/2} - \frac{1+\nu}{3}\cdot\frac{\nu-2}{4}\cdot\frac{\nu-3}{5}\cdot\frac{\nu+2}{6}\cdot\frac{\nu+3}{7}\cdot \\ & \left(\frac{1}{r_{j+3/2}\ r_{j+5/2}} - \frac{5}{r_{j+3/2}} + 10 - 10\ r_{j+1/2} + 5\ r_{j+1/2}\ r_{j-1/2}\right. \\ & \left. - r_{j+1/2}\ r_{j-1/2}\ r_{j-3/2}\right)\end{aligned} \tag{13}$$

Approximation: o-th order **OSo** scheme

High-order One step scheme (L-W): [Daru & Tenaud 2001, 2004]

- Developed up to 11-th accuracy order (non-linear scalar)
- Control of the dissipation in time and space
- Stencil of OSp = $p + 2$ grid-points: rather compact, more than method-of-line approaches (RK-WENO, for instance)
- $CFL = 1 \Rightarrow$ exact solution is recovered

Spectral property: **OS7** scheme

Von Neumann Analysis:

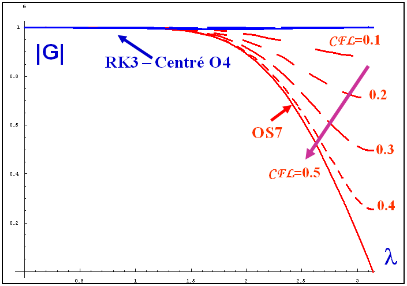

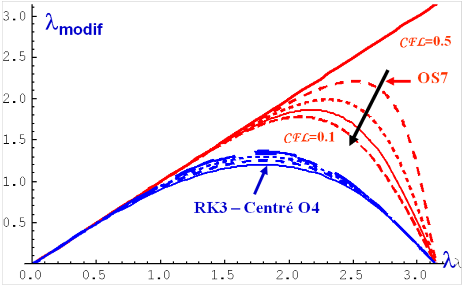

Spurious oscillations in the vicinity of discontinuities

$$F^o_{j+1/2} = f^n_j + \Phi^o_{j+1/2}\frac{(1-\nu)}{2}(f^n_{j+1} - f^n_j)$$

TVD Harten's criteria for one-step schemes:

$$-\frac{2}{\nu} \leq \Phi_{j-1/2} - \Phi_{j+1/2}/r_{j+1/2} \leq \frac{2}{1-\nu}$$

Upper bound of the TVD constraint: ($\Phi = 0$ for $r < 0$)

$$\Phi^{o-TVD}_{j+1/2} = \max(0, \min(\frac{2}{1-\nu}, \ \Phi^o_{j+1/2}\ , \ \frac{2\ r_{j+1/2}}{\nu})). \qquad (14)$$

Resulting scheme: $o-th$ order accurate almost everywhere, except around extrema and discontinuities ($\hookrightarrow 1^{st}$ order)

Geometrical interpretation of the TVD conditions

Recast Flux for the lower and the upper TVD limits

$$F_{j+1/2} = f_j^n + \gamma^+ (f_{j+1}^n - f_j^n) \quad \text{with} \quad \gamma^+ = \Phi_{j+1/2} \, \frac{(1-\nu)}{2}$$

$$F_{j+1/2} = f_j^n + \gamma^- (f_j^{ul} - f_j^n)$$

$$\text{with} \quad f_j^{ul} = f_j^n + \frac{1-\nu}{\nu}(f_j^n - f_{j-1}^n) \ \text{ and } \ \gamma^- = \Phi_{j+1/2} \, \frac{\nu}{2\, r_{j+1/2}}$$

TVD constraints

$$\begin{cases} 0 \le \Phi_{j+1/2} \le \dfrac{2}{1-\nu} \\ 0 \le \Phi_{j+1/2} \le \dfrac{2\, r_{j+1/2}}{\nu} \end{cases} \Leftrightarrow F_{j+1/2} \in [f_j^n, f_{j+1}^n] \cap [f_j^n, f_j^{ul}]. \qquad (15)$$

Clipping near extrema $\Rightarrow$ enlarge TVD constraints $\rightarrow$ Monotonicity Preserving constraints [A. Suresh & H.T. Huynh, JCP **136**(1997)]

Monotonicity Preserving constraints

Defining $[f^1, f^2, ..., f^k] = [min(f^1, f^2, ..., f^k), max(f^1, f^2, ..., f^k)]$

TVD enlargement

$[f_j^n, f_{j+1}^n]$ enlarged to $[f_j^n, f_{j+1}^n, f_j^{md}]$; $f_j^{md} = \frac{1}{2}(f_j^n + f_{j+1}^n) - \frac{1}{2} d_{j+1/2}$

$[f_j^n, f_j^{ul}]$ enlarged to $[f_j^n, f_j^{ul}, f_j^{lc}]$; $f_j^{lc} = f_j^n + \frac{1}{2}(f_j^n - f_{j-1}^n) + \frac{1}{2}\frac{1-\nu}{\nu} d_{j-1/2}$

$$\text{with} \left\{ \begin{array}{l} d_{j+1/2} = d_{j+1/2}^{MM} = minmod(d_j, d_{j+1}) \\ or \\ d_{j+1/2} = d_{j+1/2}^{M4} = minmod(4d_j - d_{j+1}, 4d_{j+1} - d_j, d_j, d_{j+1}) \end{array} \right.$$

Measure of local curvature $d_j = f_{j+1}^n - 2f_j^n + f_{j-1}^n$

Monotonicity Preserving schemes (OSMP)

Geometrical interpretation of MP constraints:

$$F_{j+1/2} \in [f_j^n, f_{j+1}^n, f_j^{md}] \cap [f_j^n, f_j^{ul}, f_j^{lc}]$$

MP criteria, in the TVD framework: [Daru & Tenaud, JCP **193** (2004)]

$$\Phi^{o-MP} = max(\Phi^{min}, min(\Phi^{o}, \Phi^{max}))$$

where $$\begin{cases} \Phi^{min} = max(min(0, \Phi^{md}), min(0, \frac{2r}{\nu}, \Phi^{lc})) \\ \Phi^{max} = min(max(\frac{2}{1-\nu}, \Phi^{md}), max(0, \frac{2r}{\nu}, \Phi^{lc})) \end{cases}$$

Extension to system of equations

k-wave characteristics

$$F_{j+1/2} = F^{Roe}_{j+1/2} + \frac{1}{2}\sum_k (\Phi^o_k(1-|\nu_k|)\delta|f_k|\mathbf{r}_k)_{j+1/2}$$

with

$$F^{Roe}_{j+1/2} = \frac{1}{2}(f_j + f_{j+1}) - \frac{1}{2}\sum_k (\delta|f_k|\mathbf{r}_k)_{j+1/2}$$

and

$$\delta|f_k| = |\lambda_k|\delta\alpha_k$$

$\delta\alpha_k$ is the k-th Riemann invariant

λ_k and $\mathbf{r}_k$ eigenvalues and right eigenvectors of the Roe-average of $\dfrac{df}{dw}$,

local CFL : $\nu_k = \frac{\delta t}{\delta x}\lambda_k$.

Extension to multi-D

Strang directional splitting:

$$w_j^{n+1} = L_{\delta x}(\delta t/2) L_{\delta y}(\delta t) L_{\delta x}(\delta t/2).w_j^n$$

Splitting implementation: symmetry recovers

$$w_j^{n+2} = L_{\delta x}(\delta t) L_{\delta y}(\delta t) L_{\delta y}(\delta t) L_{\delta x}(\delta t).w_j^n$$

$$\begin{aligned} w_j^{n+6} = \quad & (L_{\delta x} L_{\delta y} L_{\delta z})(L_{\delta x} L_{\delta z} L_{\delta y})(L_{\delta y} L_{\delta z} L_{\delta x}) \\ & (L_{\delta y} L_{\delta x} L_{\delta z})(L_{\delta z} L_{\delta y} L_{\delta x})(L_{\delta z} L_{\delta x} L_{\delta y}).w_j^n \end{aligned}$$

- Easily preserve Monotonicity in Multi-D
- Generally the splitting is 2nd order, only !
- However, OSMP gives a very low error level.

Scalar 1D test-case

$$\begin{cases} u_t + u_x = 0.\ t \leq 0; x \in [-1, 1] \\ u_0(x) = Sin^4(2.\pi.x) \end{cases}$$

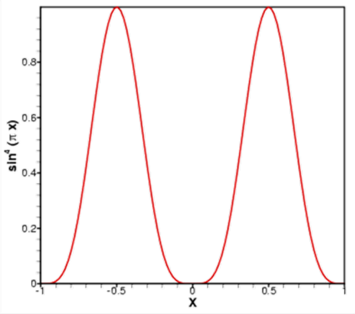

Method	Number of grid points	L_1 error	L_1 order
OS 7	20	$5.16494\ 10^{-3}$	
OS MP 7	40	$5.66989\ 10^{-5}$	6.51
$d_{j+1/2} = d^{\mathrm{MM}}_{j+1/2}$	80	$4.74407\ 10^{-7}$	6.90
	160	$3.76700\ 10^{-9}$	6.98
	320	$2.95501\ 10^{-11}$	6.99
OS MP 7	20	$5.08530\ 10^{-3}$	
$d_{j+1/2} = d^{\mathrm{M4}}_{j+1/2}$	40	$5.67752\ 10^{-5}$	6.48
	80	$6.84954\ 10^{-7}$	6.37
	160	$2.19588\ 10^{-8}$	4.96
	320	$1.33241\ 10^{-9}$	4.04
OS TVD 7	20	$2.13730\ 10^{-2}$	
	40	$3.85456\ 10^{-3}$	2.47
	80	$7.78303\ 10^{-4}$	2.31
	160	$1.47891\ 10^{-4}$	2.40
	320	$2.73871\ 10^{-5}$	2.43

Euler 2D test-case: Vortex advection

Strong vortex propagated at 45° by a supersonic flow:

$$(\delta u, \delta v) = \frac{\varepsilon}{2\pi} e^{0.5(1-r^2)}(-y, x) \;\; ; \;\; \delta T = -\frac{(\gamma-1)\varepsilon^2}{8\pi^2} e^{0.5(1-r^2)} \;\; ; \;\; \delta S = 0.$$

$\varepsilon = 5$; $(\rho, u, v, P) = (1, 1, 1, 1)$ and $(x \times y) = [-5, 5] \times [-5, 5]$

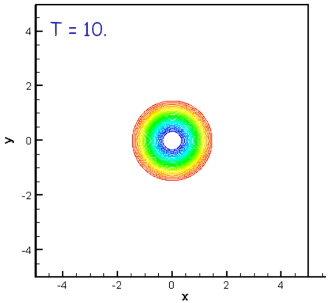

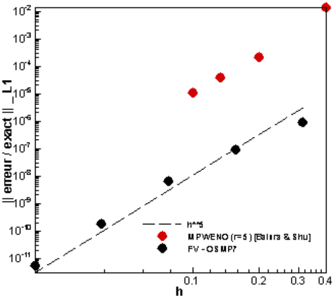

Navier-Stokes 2D test-case: viscous shock tube

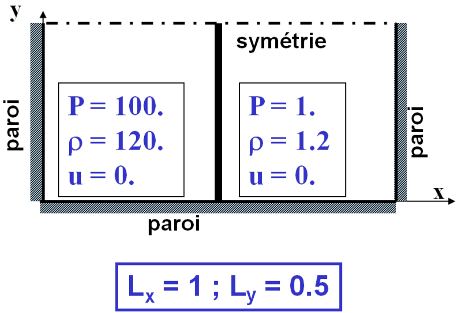

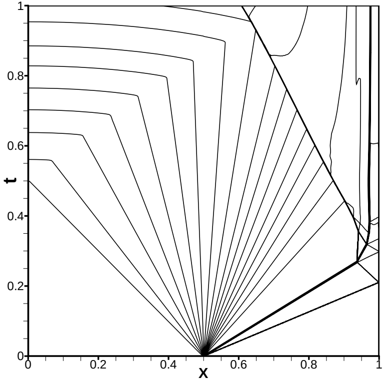

Navier-Stokes 2D test-case: viscous shock tube

Isocontours of $|\nabla\rho|$ at t=1

Re = 200 (1000 × 500)

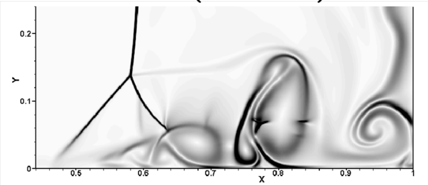

Re = 500 (1500 × 750)

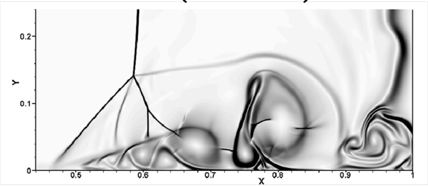

Re = 750 (2000 × 1000)

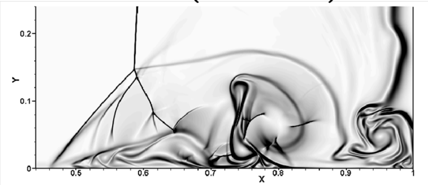

Re = 1000 (4000 × 2000)

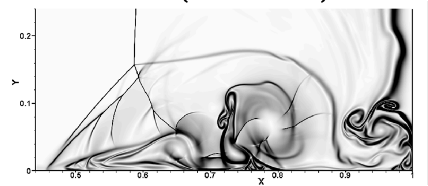

Navier-Stokes 2D test-case: viscous shock tube

Distribution of ρ along the lower wall at t=1

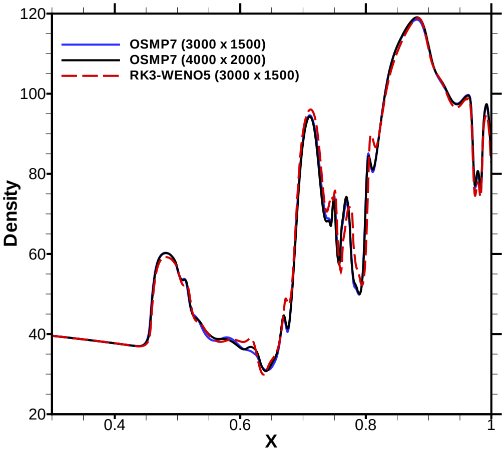

Overview

- System of equations;
- Numerical approximation **OSMPx** [V. Daru & C. Tenaud, 2001, 2004];
  - Lax-Wendroff approach;
  - Shock capturing features (TVD, MP);
- Adaptive MultiResolution technique [A. Harten, 1994 ; A. Cohen, 2003];
  - Multiscale decomposition;
  - Adaptive MR formalism: wavelet basis;
- Couple OSMPx / adaptive MR. Influence on accuracy, CPU time consumption, memory usage, evaluated on well known test-cases:
  - Hyperbolic conservation laws: linear and nonlinear scalar transport equation,
  - Euler and Navier-Stokes solutions in 1-, 2- and 3-D.
- Conclusion and prospect.

Nested grids

Dyadic grids: Grid level : $l \in [0, L]$

Cell referenced by position and grid-level:(j, l)

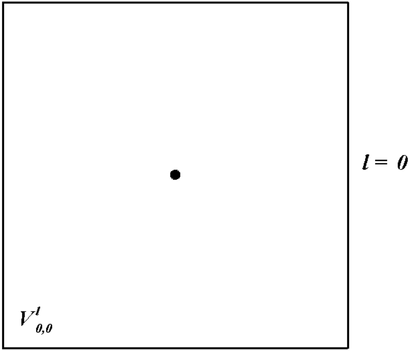

Nested grids

Dyadic grids: Grid level : $l \in [0, L]$

Cell referenced by position and grid-level:(j, l)

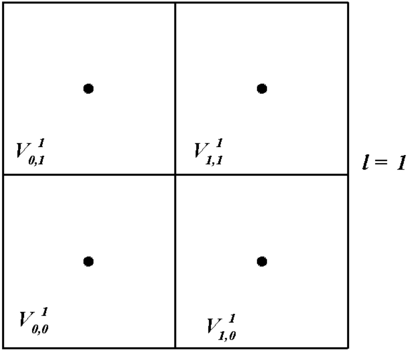

Nested grids

Dyadic grids: Grid level : $l \in [0, L]$

Cell referenced by position and grid-level:(j, l)

$$(j, l) \rightarrow (2j, l+1)\ ,\ (2j+1, l+1)$$

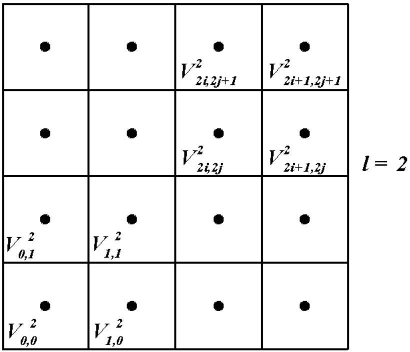

Nested grids

Dyadic grids: Grid level : $l \in [0, L]$

$$\Omega = \bigcup_{j \in I_l} V_j^l \quad \text{with} \quad \left| V_j^l \bigcap V_k^l \right| = 0,$$

for $j \neq k$; $j, k \in I_l$.

Refinement process:

$$V_j^l = \bigcup_{p \in \mathcal{C}_j^l} V_p^{l+1},$$

$\mathcal{C}_j^l$ set of *chidren* indexes of V_j^l.

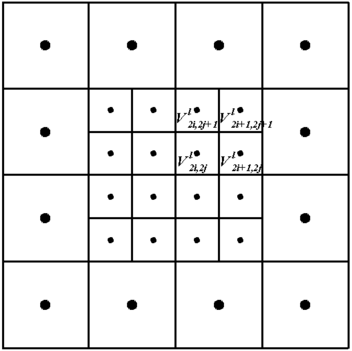

$l = \ldots$

Tree data Structure

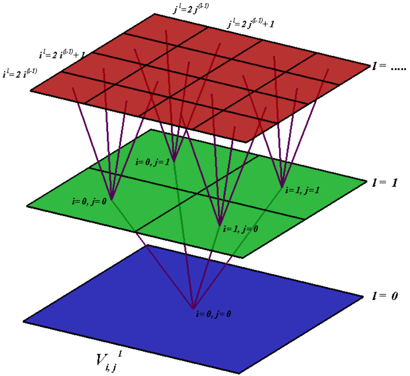

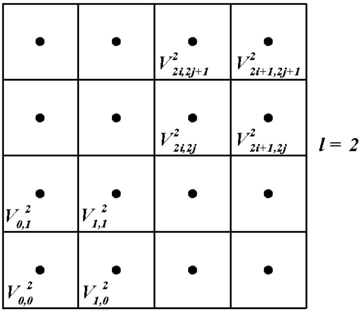

Terminology: *father* $(j/2, l-1)$; *children* $(2j, l+1)$, $(2j+1, l+1)$; *cousin* $(j+1, l)$, $(j-1, l)$
leaves are upper elements (with no *child*)

Projection operator:

$\mathbf{P}_{l+1\to l}$: compute $\mathbf{v}_j^l$ knowing *children*-cells $\mathbf{v}_{2j}^{l+1}$, $\mathbf{v}_{2j+1}^{l+1}, \dots$

Nested grid: operator is *exact* and *unique* [A. Cohen *et al.*(2000)]:

Assuming cell average as: $\left(\mathbf{v}_j^l\right)^n = \frac{1}{|V_j^l|} \int_{V_j^l} \mathbf{w}(\mathbf{x}, n\,\delta t)\, d\mathbf{x}$

Projection operator:

$$\mathbf{P}_{l+1\to l}: \quad \mathbf{v}_j^l = \frac{1}{|V_j^l|} \sum_{p\in\mathcal{C}_j^l} |V_p^{l+1}|\; v_p^{l+1};$$

$\mathcal{C}_j^l$ index set of the $2^{N_{dim}}$ *children*-cells at grid-level $l+1$, for current cell V_j^l.

Prediction operator:

$\mathbf{P}_{l\to l+1}$: maps $\mathbf{v}^l$ to an approximate value $\hat{\mathbf{v}}^{l+1}$ of $\mathbf{v}^{l+1}$.

$\mathbf{P}_{l\to l+1}$ is not unique and **prediction** needs to be:

- *local*; interpolation stencil must contain the *parent*-cell and its nearest neighbors in each direction [A. Cohen *et al.*(2000), M. Postel (2001)].
- *consistent with the projection* operator, *i.e.* $\mathbf{P}_{l+1\to l} \circ \mathbf{P}_{l\to l+1} = Id$.
  Conservativity:
  $$|V_j^l|\ v_j^l = \sum_{p\in\mathcal{C}_j^l} |V_p^{l+1}|\ \hat{v}_p^{l+1}$$
- *linear* (not mandatory...) $\rightarrow$ simplicity of the numerical analysis.
  Information on non-linear operator found in [F. Anràndiga *et al.*(1999)]

Prediction operator: interpolation

Prediction interpolation: centered linear polynomial

$$\mathbf{P}_{l\to l+1} : \begin{cases} \hat{v}_{2j}^{l+1} = v_j^l + \sum_{q=1}^{s} \xi_q \left(v_{j+q}^l - v_{j-q}^l \right), \\ \hat{v}_{2j+1}^{l+1} = v_j^l - \sum_{q=1}^{s} \xi_q \left(v_{j+q}^l - v_{j-q}^l \right), \end{cases}$$

Coefficients of centered linear polynomial:

order (o)	s	ξ_1	ξ_2
0	0	0	0
2	1	$\frac{-1}{8}$	0
4	2	$\frac{-22}{128}$	$\frac{3}{128}$

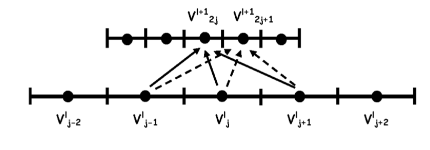

for $s = 1$

Prediction operator: multi-D interpolations

Extension to multidimensional Cartesian grids:

Tensorial product of 1-D operator [B.L. Bihari & A. Harten (1997), O. Roussel *et al.*(2003)].

2D-interpolation

$$\hat{v}^{l+1}_{2j+p,2k+q} = v^l_{j,k} + (-1)^p \; Q^s(j;\mathbf{v}^l_{\cdot,k}) + (-1)^q \; Q^s(k;\mathbf{v}^l_{j,\cdot}) - (-1)^{(p+q)} \; Q^s_2(j,k;\mathbf{v}^l),$$

with $p, q \in [0,1]$ and:

$$Q^s\left(j;v^l\right) = \sum_{q=1}^{s} \xi_q \left(v^l_{j+q} - v^l_{j-q}\right),$$

$$Q^s_2\left(j,k;\mathbf{v}^l\right) = \sum_{a=1}^{s} \xi_a \sum_{b=1}^{s} \xi_b \left(v^l_{j+a,k+b} - v^l_{j-a,k+b} - v^l_{j-a,k+b} + v^l_{j-a,k-b}\right).$$

Prediction operator: *details*

prediction error: *details* (d_j^l)

details

$$\mathbf{d}_j^l = \mathbf{v}_j^l - \hat{\mathbf{v}}_j^l.$$

Consistency assumption [A. Harten (1995)]: $\sum_{p \in \mathcal{C}_j^l} |V_p^l| \, d_p^l = 0.$

Knowing $2^{N_{dim}}$ cell-averages $\mathbf{v}_\cdot^{l+1} \Leftrightarrow$ knowing $\mathbf{v}_j^l$ and $(2^{N_{dim}} - 1)$ $\mathbf{d}_\cdot^l$:

$$v_{2k}^{l+1} = \hat{v}_{2k}^{l+1} + d_{2k}^{l+1};$$

$$v_{2k+1}^{l+1} = \frac{|V_j^l|}{|V_{2k+1}^{l+1}|} \, v_j^l - v_{2k}^{l+1}.$$

Prediction operator: *details*

Polynomial accuracy

$$\left|\mathbf{d}^l\right| \leq C\, 2^{-l}\left|\mathbf{v}^l\right|_{L^\infty(V_j^l)}.$$

Main property for MR process:

- Solution with locally bounded *o*-th order derivatives [A. Cohen *et al.*(1992)];

$$|\mathbf{d}^l| = 0.$$

- Decay with 2^{-l} for solutions smooth enough;
- Significantly high *detail* values within singularities.

Multiresolution transform:

$$\mathbf{D}^l = \left\{ d_j^l,\ 0 \leq j \leq N_l \right\},\quad \text{with } N_l = (2^{N_{dim}} - 1)\ 2^{N_{dim}(l-1)}$$

$$\mathbf{v}^{(l+1)} \longmapsto \left(\mathbf{v}^l,\ \mathbf{D}^{l+1} \right).$$

One to one transformation: from *leaves* down to the root

$$\mathcal{M} : \mathbf{v}^L \longmapsto \left(\mathbf{v}^0, \mathbf{D}^1, \ldots, \mathbf{D}^L \right) = \mathbf{M}^L.$$

$$\begin{tikzcd}
\bar{v}_L \arrow[r, leftrightarrow] \arrow[dr, leftrightarrow] & \bar{v}_{L-1} \arrow[r, leftrightarrow] \arrow[dr, leftrightarrow] & \bar{v}_{L-2} \arrow[r, leftrightarrow] \arrow[dr, leftrightarrow] & \cdots \arrow[r, leftrightarrow] \arrow[dr, leftrightarrow] & \bar{v}_1 \arrow[r, leftrightarrow] \arrow[dr, leftrightarrow] & \bar{v}_0 \\
 & d_{L-1} & d_{L-2} & \cdots & d_1 & d_0
\end{tikzcd}$$

Thresholding:

Solution known by $\left(\mathbf{v}^0, \mathbf{D}^1, \ldots, \mathbf{D}^L\right) = \mathbf{M}^L$;

Algorithm 1: Predictive Harten's thresholding

For $l = L - 1$ down to 1, with $\varepsilon_l = 2^{N_{ndim}\cdot(l-L)}\ \varepsilon$, **Do**

for $j \in I_l$, **do**

- **If** *(i)* $\dfrac{\left|d_j^l\right|_{L_1}}{\max_j \left|d_j^l\right|} < \varepsilon_l$, **then**

  Assuming solution slowly propagates at a finite speed:

  1. $d_j^l = 0$;
  2. $\widehat{t}_{2j}^{l+1} = \text{ false and } \widehat{t}_{2j+1}^{l+1} = \text{ false } \longmapsto$ discarded;

- **Else** $d_j^l \in \mathbf{D}^l$ and $\widehat{t}_{2j+q}^{l+1} = \text{ true with } -K \leq q \leq K+1$;

  "K" = maximal speed of propagation: *i.e.* K chosen as flux stencil width.

  $K = 1$ in most cases, coherent with *CFL*-condition.

  - . . .

Thresholding:

Algorithm 3 (next): Predictive Harten's thresholding

- **Else** $d_j^l \in \mathbf{D}^l$ and $\widehat{t}_{2j+q}^{l+1} = \text{ true }$ with $-K \leq q \leq K+1$;
  - Foresight discontinuity formation: assume accuracy loss predicted by *details* on coarse grid-levels.
  - **If** *(ii)* $\dfrac{\left|d_j^l\right|_{L_1}}{\max_j \left|d_j^l\right|} \geq 2^{(2.p)}\ \varepsilon_l$, **then**
    - **if** $l \neq L-1$, **then**
      New grid-level locally created: $\widehat{t}_{2q}^{l+2} = \text{ true }$ and $\widehat{t}_{2q+1}^{l+2} = \text{ true }$, with $2j-K \leq q \leq 2j+1+K$;
    - **end if**
      p parameter related to regularity analysis,
      $1 \leq p \leq o-1$ for 1D, $p = o+1, o+2$ for multi-D
  - **End If**
- **End If**

End for

End For

Thresholding: control

Approximation MR operator: $\mathcal{A}_{\Lambda_{\varepsilon_l}}$

$$\|\mathbf{v}^L - \mathcal{A}_{\Lambda_{\varepsilon_l}}\mathbf{v}^L\| = C \sum_{|\mathbf{d}^l|<\varepsilon_l} |\mathbf{d}^l|\, 2^{-N_{dim} l}$$

Control of the thresholding effect: Harten (1994):

$$\varepsilon_l = 2^{N_{ndim}.(l-L)}\ \varepsilon$$

Knowing $\varepsilon : \|\mathbf{v}^L - \mathcal{A}_{\Lambda_{\varepsilon_l}}\mathbf{v}^L\| \leq C\varepsilon$

Conservativity: Virtual cells

Numerical flux evaluation at cell interfaces: conservative property.

- *virtual*-cells are added to the tree. Solution **is not integrated** on *virtual*-cells
- Evaluate solution on *virtual*-cells by **decoding**.
- Flux evaluation at the highest grid level

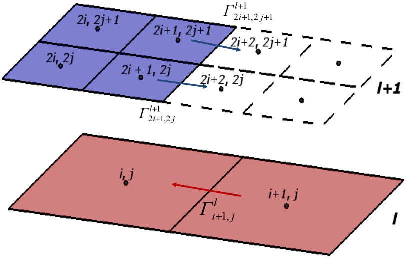

$$F^l_{i,j\to i+1,j}\,\Gamma^l_{i,j\to i+1,j} = \sum_{q=2j}^{2j+1} F^{l+1}_{2i+1,q\to 2i+2,q}\,\Gamma^{l+1}_{2i+1,q\to 2i+2,q}.$$

Summing up the MR procedure

- Cell-average values of solution ($\mathbf{v}_j^L$) known on *leaves*;

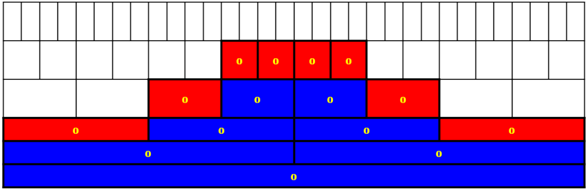

Summing up the MR procedure

- Cell-average values of solution ($\mathbf{v}_j^L$) known on *leaves*;
- Projection: $\mathbf{v}_j^l = \dfrac{1}{|V_j^l|} \sum_{p \in \mathcal{C}_j^l} |V_p^{l+1}| \, \mathbf{v}_p^{l+1}$;

$l = L - 1$ **down to** 0

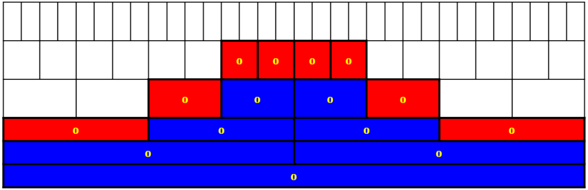

Summing up the MR procedure

- Cell-average values of solution ($\mathbf{v}_j^L$) known on *leaves*;
- Projection: $\mathbf{v}_j^l = \dfrac{1}{|V_j^l|} \displaystyle\sum_{p \in \mathcal{C}_j^l} |V_p^{l+1}| \, \mathbf{v}_p^{l+1}$;
- Encoding details: $\hat{v}_{2j}^{l+1} = v_j^l + \sum_{q=1}^{s} \xi_q \left(v_{j+q}^l - v_{j-q}^l \right)$
  $d_{2j}^{l+1} = v_{2j}^{l+1} - \hat{v}_{2j}^{l+1}$

$l = 0$ **up to** $L - 1$

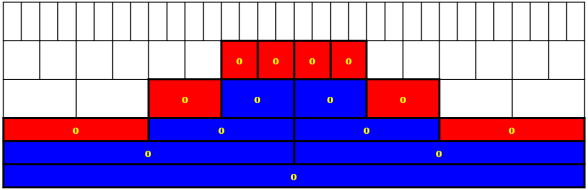

Summing up the MR procedure (next)

- Thresholding: $\left|\mathbf{d}^l\right|_{L_1} < \varepsilon_l$;

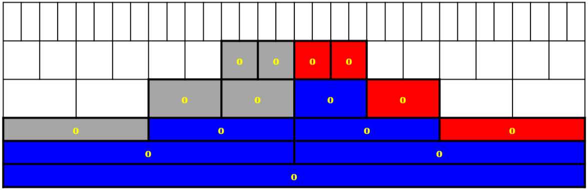

Summing up the MR procedure (next)

- Thresholding: $\left|\mathbf{d}^l\right|_{L_1} < \varepsilon_l$;
- Enlarge the tree for foreseeing discontinuity: $\left|\mathbf{d}^l\right|_{L_1} \geq \varepsilon_l$ and $\left|\mathbf{d}^l\right|_{L_1} \geq 2^p\ \varepsilon_l$

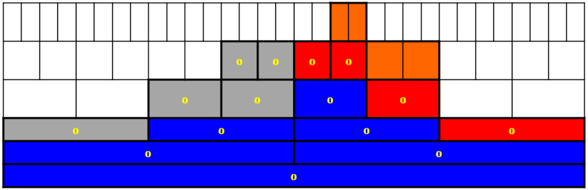

Summing up the MR procedure (next)

- Thresholding: $\left|\mathbf{d}^l\right|_{L_1} < \varepsilon_l$;
- Enlarge the tree for foreseeing discontinuity: $\left|\mathbf{d}^l\right|_{L_1} \geq \varepsilon_l$ and
  $\left|\mathbf{d}^l\right|_{L_1} \geq 2^p\, \varepsilon_l$
- Building graded tree:
  if $(j,l) \in \widetilde{\Lambda}_{\varepsilon_l}$ then $(j/2+q, l-1) \in \widetilde{\Lambda}_{\varepsilon_l}$; $q \in [-s,+s]$

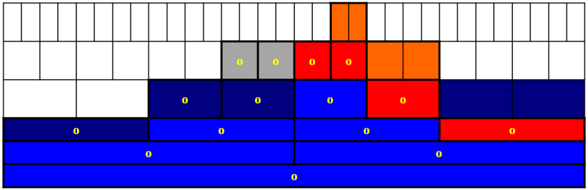

Summing up the MR procedure (next)

- Thresholding: $\left|\mathbf{d}^l\right|_{L_1} < \varepsilon_l$;
- Enlarge the tree for foreseeing discontinuity: $\left|\mathbf{d}^l\right|_{L_1} \geq \varepsilon_l$ and
  $$\left|\mathbf{d}^l\right|_{L_1} \geq 2^p\, \varepsilon_l$$
- Building graded tree:
  if $(j,l) \in \widetilde{\Lambda}_{\varepsilon_l}$ then $(j/2+q, l-1) \in \widetilde{\Lambda}_{\varepsilon_l}$; $q \in [-s,+s]$
- Add virtual *leaves* for flux conservation

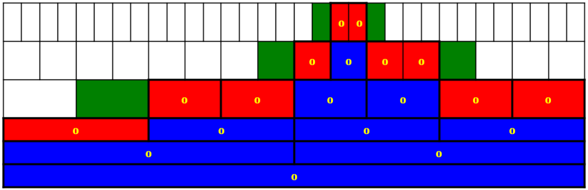

Test-Cases

- Codes based on Fortran95;
- Objective: illustrate influence of MR parameters (ε, s, L, ...) on performances (accuracy, CPU time, Memory compression);
- Several examples:
  - Solving nonlinear scalar transport equation: 1D Burger equation;
  - Solving a 2D linear scalar transport equation;
  - Solving Euler and Navier-Stokes problems:
    - 2D Vortex advection;
    - 2D Shock / hot spot interaction;
    - 2D viscous shock tube problem;
    - 3D Euler shock tube.

Solving 1D nonlinear scalar advection with MR procedure

- The 1D burger equation:

$$\frac{\partial u}{\partial t} + \nabla \cdot f(u) = 0, \quad \text{in } \Omega, \quad \text{with } f(u) = \frac{1}{2}\, u^2.$$

- Initial solution:

$$u(x,0) = -V_{left}\ \sin(2.\ \pi\ x)\,;\ x \in [-1,1],$$

where V_{left} is an input value.

- Periodic boundary conditions:

$$u(-1,t) = u(1,t)$$

- Solved by using the One-Step Monotonicity-Preserving scheme (OSMP7) [Daru & Tenaud (2004, 2009)].

1D Burger equation with MR procedure: Solution

Solutions obtained with 10 grid levels ($N = 1024$ **grid points on the finest grid), with** $s = 1$ **and** $\varepsilon = 10^{-2}$.

$$t = 0.$$

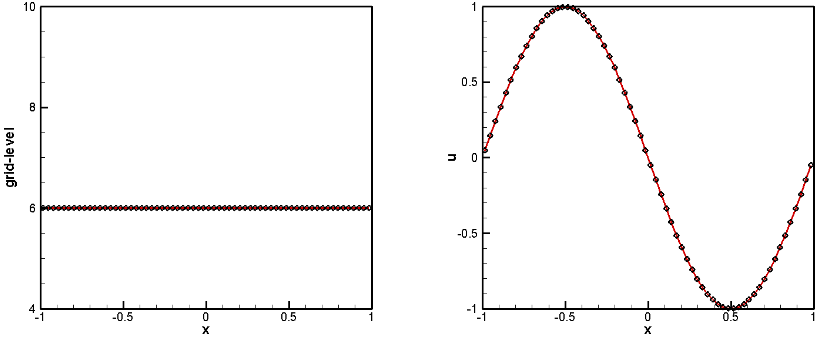

1D Burger equation with MR procedure: Solution

Solutions obtained with 10 grid levels ($N = 1024$ **grid points on the finest grid), with** $s = 1$ **and** $\varepsilon = 10^{-2}$.

$$t = 0.5$$

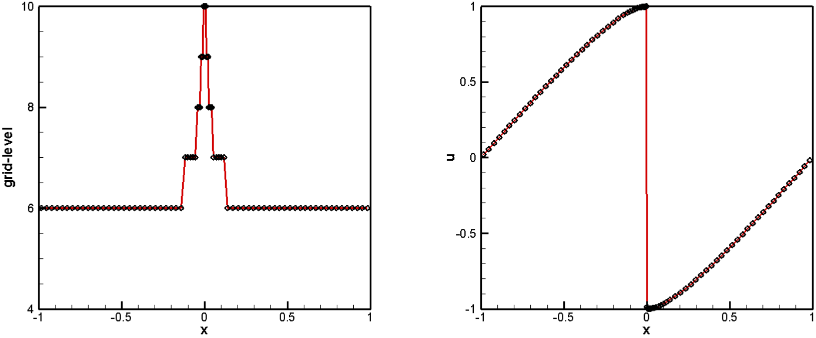

1D Burger equation with MR procedure: Perturbation error

$s = 1$

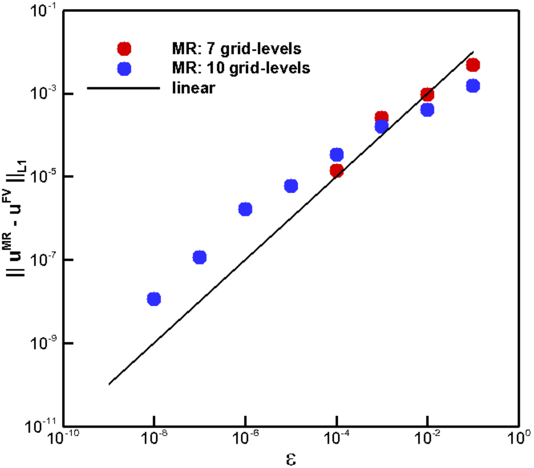

1D Burger equation with MR procedure: Efficiency

$$s = 1$$

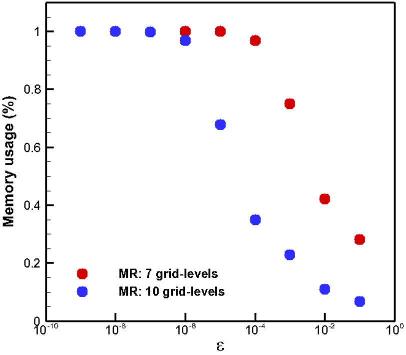

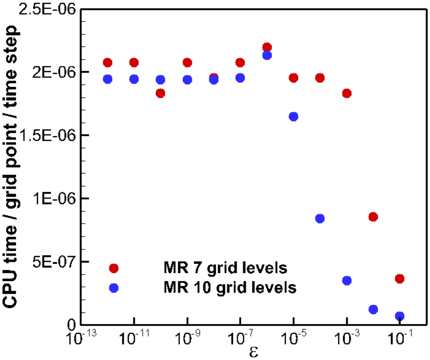

Solving 2D scalar advection with MR procedure

$$\frac{\partial u}{\partial t} + \mathbf{a} \cdot \nabla u = 0,$$

Domain: $(x \times y) \in [-1, 1] \times [-1, 1]$ with boundary conditions.

$$u_0(x) = \begin{cases} V_{left} & \text{if } \sqrt{(x - x_0)^2 + (y - y_0)^2} \leq r_0 \\ V_{right} & \text{elsewhere} \end{cases}$$

with $x_0 = 0.5$, $y_0 = 0$ and $r_0 = 0.25$

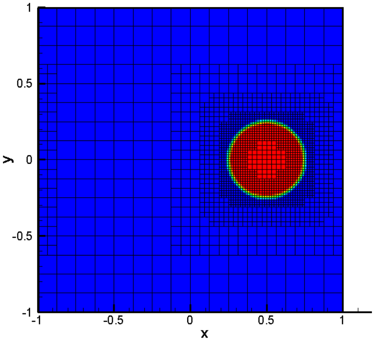

Solving 2D scalar advection with MR procedure

$$\frac{\partial u}{\partial t} + \mathbf{a} \cdot \nabla u = 0,$$

Domain: $(x \times y) \in [-1, 1] \times [-1, 1]$ with boundary conditions.

$$u_0(x) = \begin{cases} V_{left} & \text{if } \sqrt{(x - x_0)^2 + (y - y_0)^2} \leq r_0 \\ V_{right} & \text{elsewhere} \end{cases}$$

with $x_0 = 0.5$, $y_0 = 0$ and $r_0 = 0.25$

Here $\mathbf{a}$ is a vector with two components that are independent $u(\mathbf{x}, t)$:

$$\mathbf{a} = \begin{pmatrix} -y \\ +x \end{pmatrix}$$

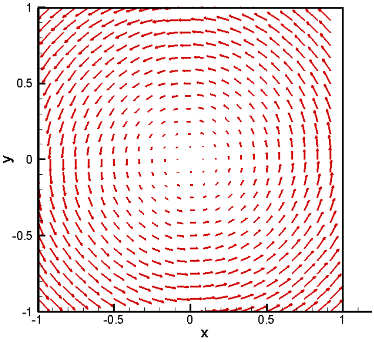

2D scalar advection: MR - 10 levels (1024×1024), $s = 1$, $\varepsilon = 10^{-3}$

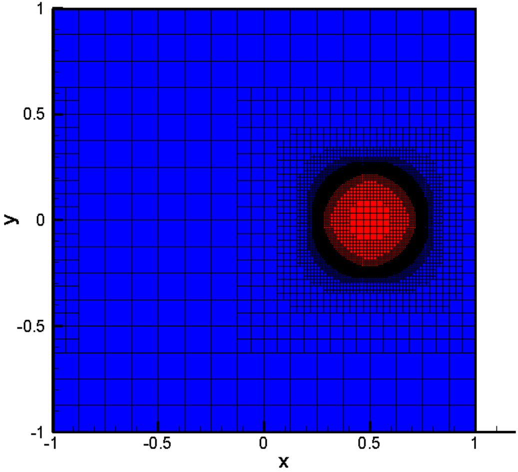

2D scalar advection: MR - 10 levels (1024×1024), $s = 1$, $\varepsilon = 10^{-3}$

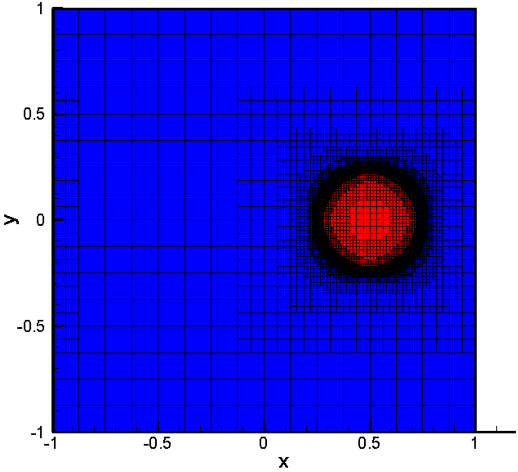

2D scalar advection with MR procedure: Perturbation error

MR on 7 grid-levels (finest grid is (128×128))

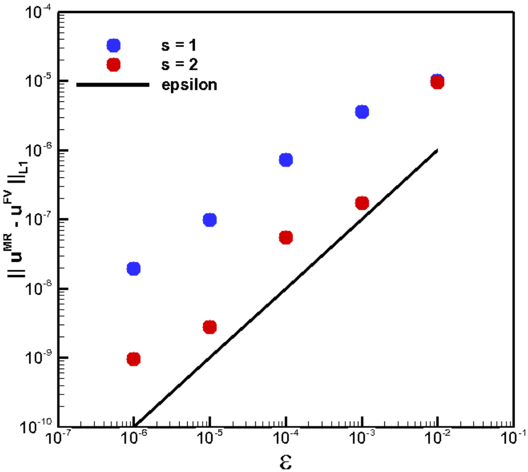

2D scalar advection with MR procedure: Efficiency

MR on 7 grid-levels (finest grid is (128×128)).

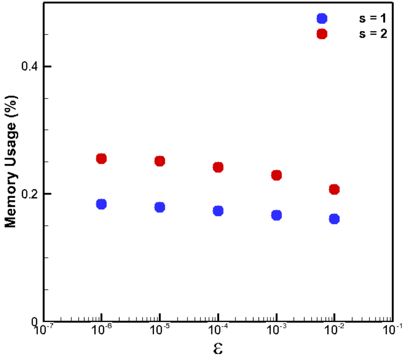

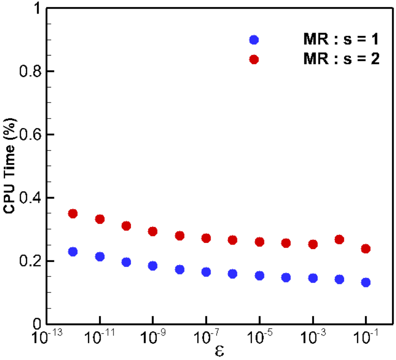

Euler 2D Vortex advection: solution

Strong vortex propagated at 45° by a supersonic flow:

$$(\delta u, \delta v) = \frac{\varepsilon}{2\pi} e^{0.5(1-r^2)}(-y, x) \;\; ; \;\; \delta T = -\frac{(\gamma-1)\varepsilon^2}{8\pi^2} e^{0.5(1-r^2)} \;\; ; \;\; \delta S = 0.$$

$\varepsilon = 5$; $(\rho, u, v, P) = (1, 1, 1, 1)$ and $(x \times y) = [-5, 5] \times [-5, 5]$

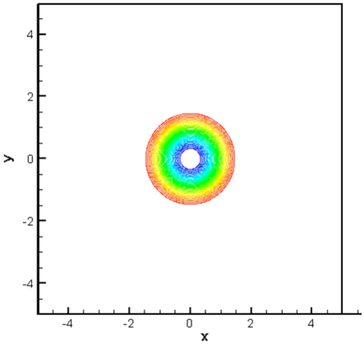

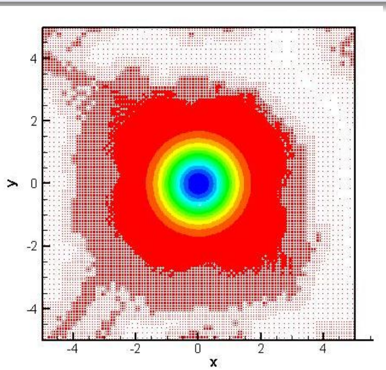

Euler 2D Vortex advection: Error analysis

Error / Exact solution

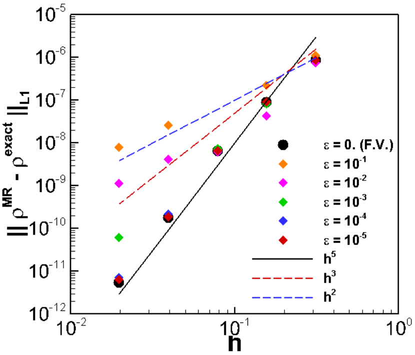

Perturbation Error $t = 10$

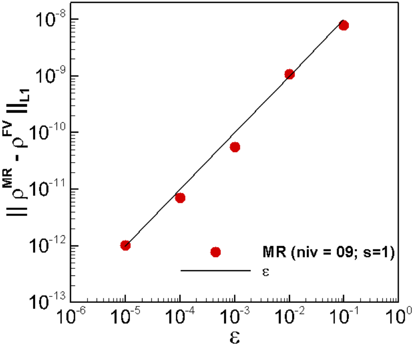

Euler 2D Vortex advection: Effciency

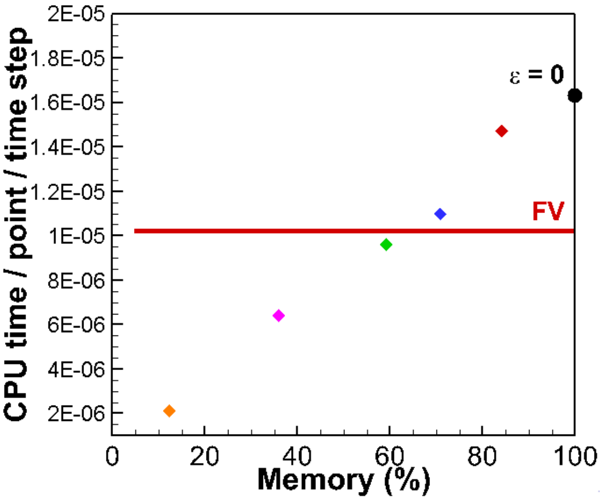

Shock Hot-spot interaction : Solution $t = 0.5$; MR $\varepsilon = 10^{-3}$, $s = 1$

$$\mathrm{M}_0 = 1.1588 \;;\; \mathrm{Re} = 2000 \;;\; \mathrm{Pr} = 0.7 \;;\; \gamma = 1.4 \;;\; (x \times y) \in [0, 2] \times [0, 1]$$

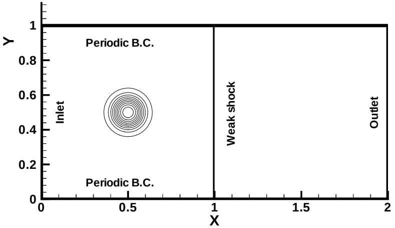

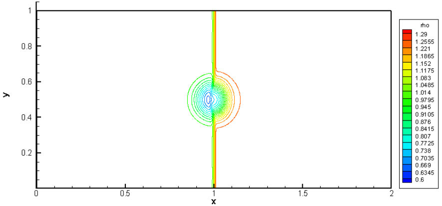

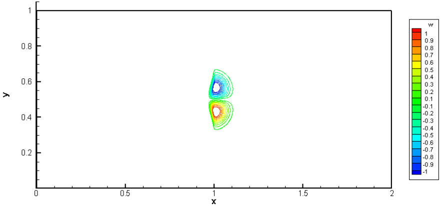

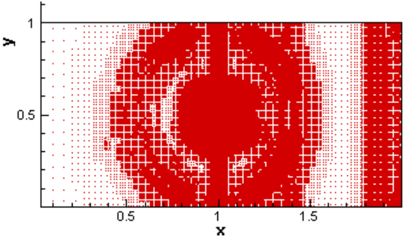

Shock Hot-spot interaction : solution $t = 1$; MR $\varepsilon = 10^{-3}$, $s = 1$

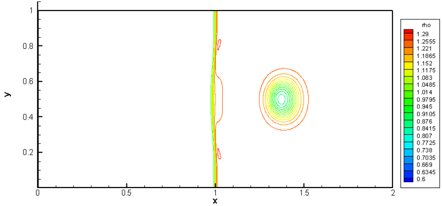

Memory compression = 79 %

CPU time ratio: t^{MR}/t^{FV} = 36 %

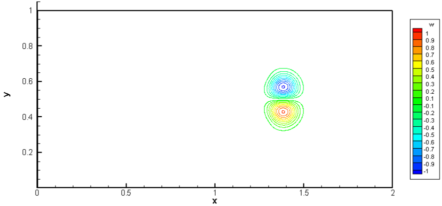

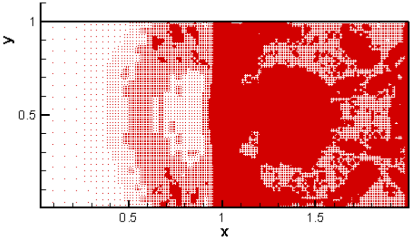

Shock Hot-spot interaction : Analysis MR $\varepsilon = 10^{-3}$, $s = 1$

$$\int_\Omega |\omega| \, d\mathbf{x}$$

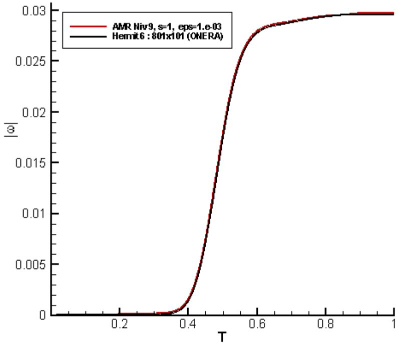

$$\int_\Omega \frac{|\nabla P \times \nabla \rho|}{\rho^2} \, d\mathbf{x}$$

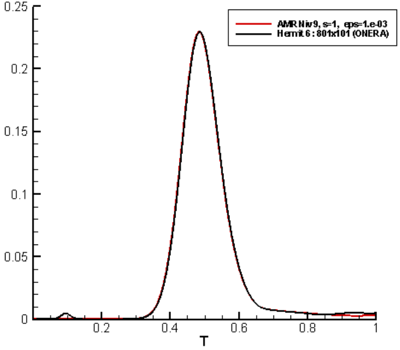

Shock Hot-spot interaction : MR Analysis 9 grid levels, $s = 1$

$$\|\rho^{MR} - \rho^{FV}\|_{L^1}$$

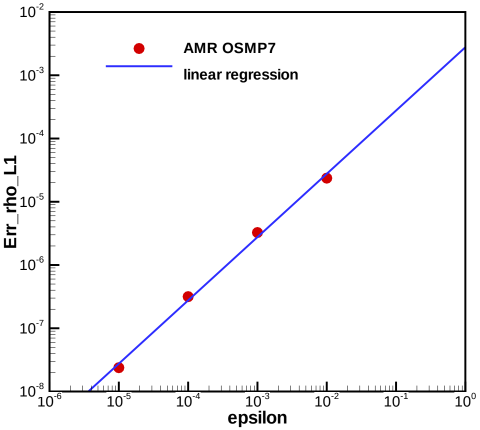

Shock Hot-spot interaction : video MR 9 grid levels, $\varepsilon = 10^{-3}$, $s = 1$

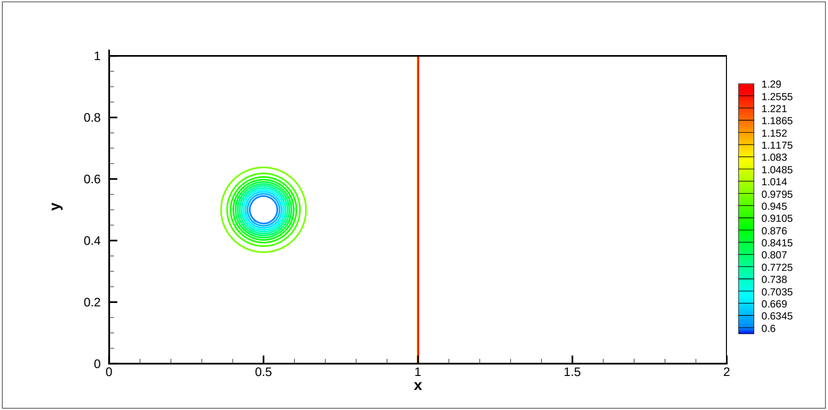

Shock Hot-spot interaction : video MR 9 grid levels, $\varepsilon = 10^{-3}$, $s = 1$

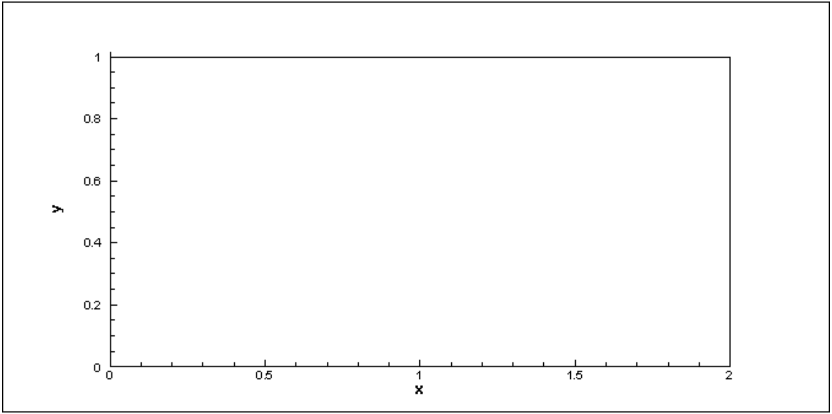

Shock Hot-spot interaction : video MR 9 grid levels, $\varepsilon = 10^{-3}$, $s = 1$

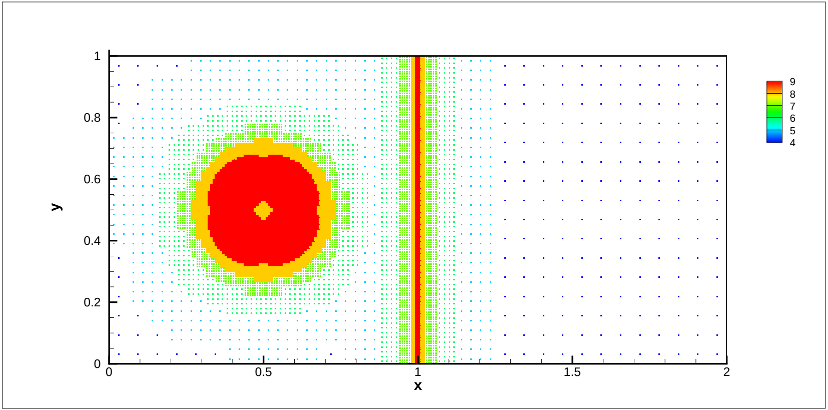

2D Viscous shock tube: MR 9 grid levels, $\varepsilon = 10^{-2}$, $s = 1$

$t = 1$

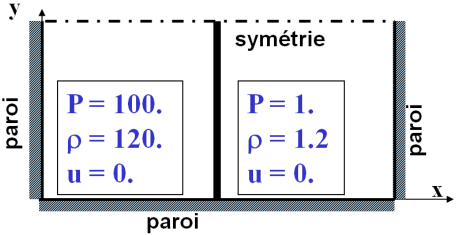

$L_x = 1$; $L_y = 0.5$

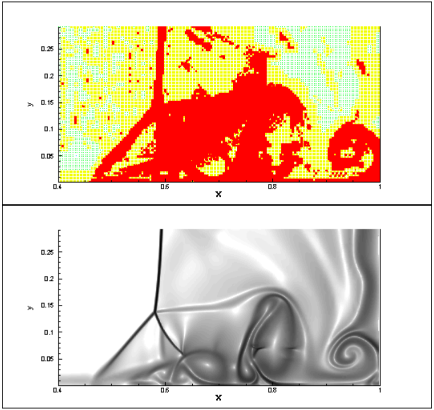

$\varepsilon = 10^{-2} \Longrightarrow$ **Memory compression = 70 %; CPU ratio: $t^{MR}/t^{FV} = 20$ %**

2D Viscous shock tube: video MR 9 grid levels, $\varepsilon = 10^{-2}$, $s = 1$

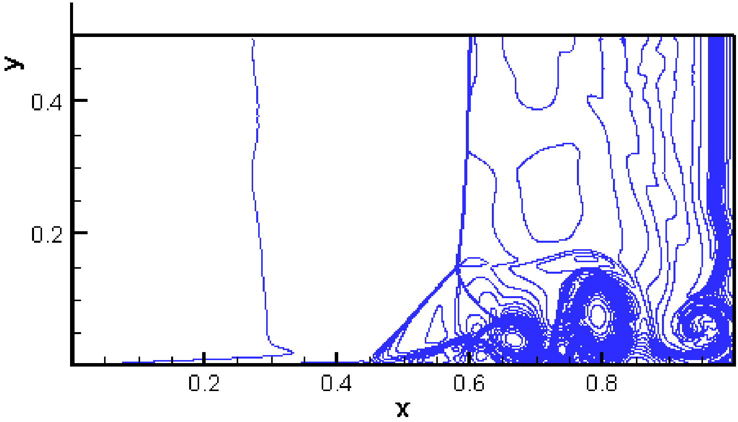

2D Viscous shock tube: video MR 9 grid levels, $\varepsilon = 10^{-2}$, $s = 1$

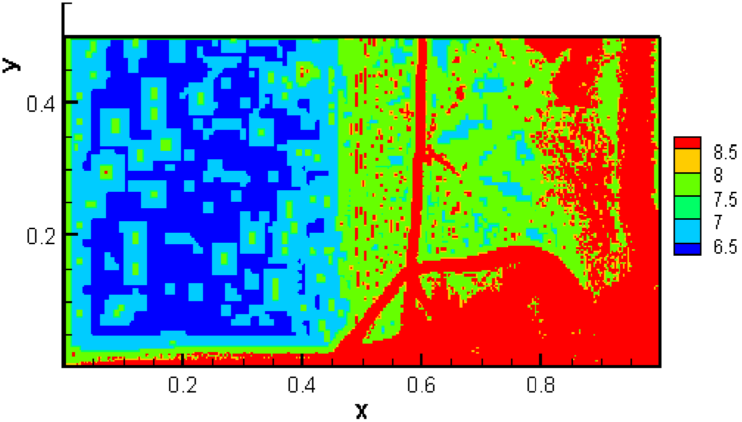

2D Viscous shock tube: MR 9 grid levels, $s = 1$

$t = 1$

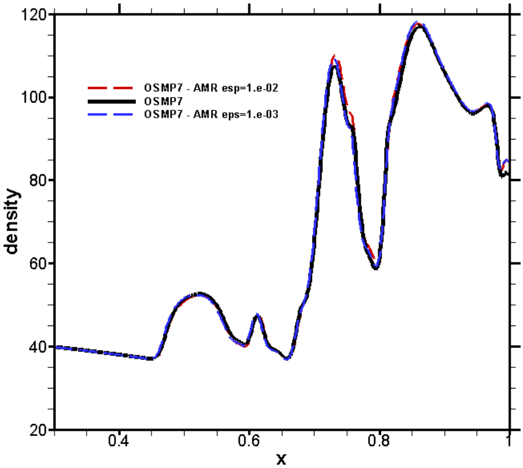

3D Euler shock tube: MR 6 levels ($190 \times 190 \times 128$), $\varepsilon = 10^{-2}$, $s = 1$

$t = 0$

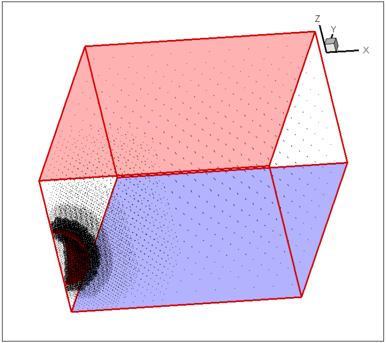

$t = 0.7$

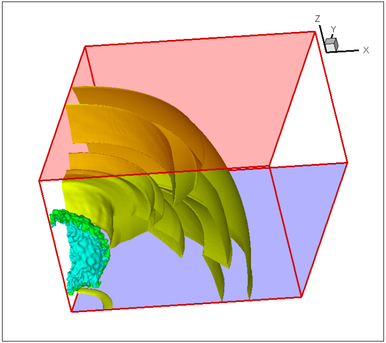

3D Euler shock tube: MR 6 levels ($190 \times 190 \times 128$), $\varepsilon = 10^{-2}$, $s = 1$

$t = 0$

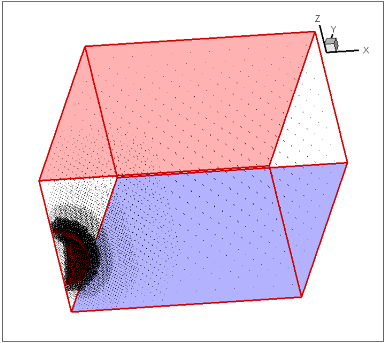

Memory compression = 99 %

$t = 0.7$

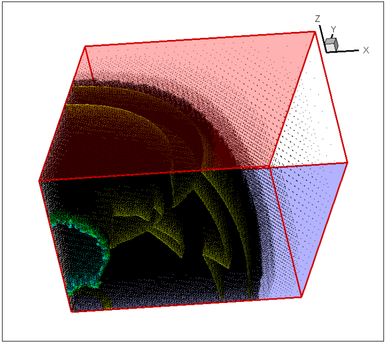

$\sim$ 50 %

CPU ratio: $t^{MR}/t^{FV} = 70$ %

3D Euler shock tube: MR 5 grid levels, $\varepsilon = 10^{-3}$, $s = 1$, $t = 0.7$

FV OSMP7 ($150 \times 150 \times 100$)

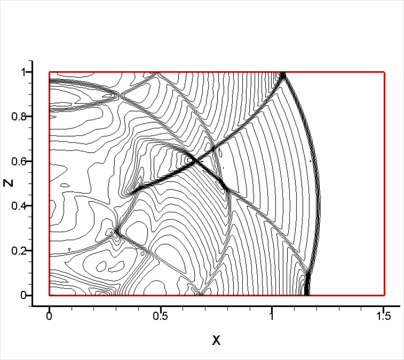

MR OSMP7 $\varepsilon = 10^{-3}$ ($160 \times 160 \times 92$)

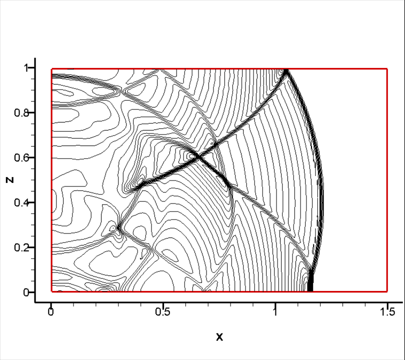

3D Euler shock tube: MR $s = 1$, $t = 0.7$

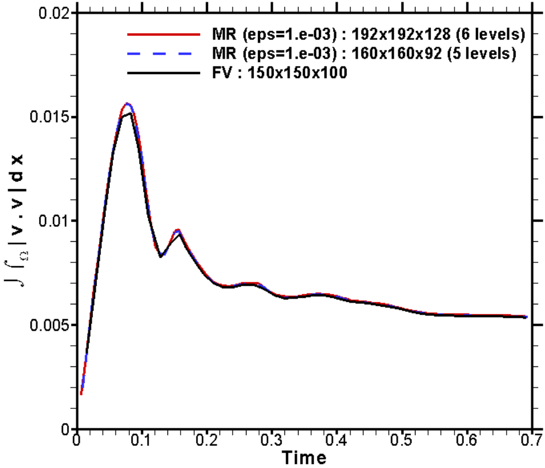

- **High-resolution Scheme:**
  - High accurate and powerfull: competitive / RK-WENO (method-of-lines);
  - Splitting allows TVD-MP constraints in Multi-D;
  - Limited to structured meshes;
- **Multiresolution technique:**
  - Attractive formalism and concept because of a priori error control;
  - Powerful but hard to handle: competitive if Mem. < 50 %;
- **future work or work in progress:**
  - Immersed Boundary conditions;
  - Combustion: Operator splitting and time step adaption (Lab. JAD, EM2C)
  - parallel algorithm (?)